

MATLAB Implementation of C^1 finite elements: Bogner-Fox-Schmit rectangle

Jan Valdman*

Institute of Mathematics, Faculty of Science,
University of South Bohemia,
Branišovská 31, 37005 České Budějovice, Czechia
and
The Czech Academy of Sciences,
Institute of Information Theory and Automation,
Pod vodárenskou věží 4, 18208 Praha 8, Czechia

jan.valdman@utia.cas.cz

May 15, 2022

Abstract

Rahman and Valdman (2013) introduced a new vectorized way to assemble finite element matrices. We utilize underlying vectorization concepts and extend MATLAB codes to implementation of Bogner-Fox-Schmit C^1 rectangular elements in 2D. Our focus is on the detailed construction of elements and simple computer demonstrations including energies evaluations and their visualizations.

Keywords: MATLAB vectorization, finite elements, energy evaluation

1 Introduction

Boundary problems with fourth order elliptic operators [3] appear in many applications including thin beams and plates and strain gradient elasticity. The weak formulation of these problems requires H^2 -conforming finite elements, leading to C^1 continuity of approximations over elements edges. This continuity condition is generally technical to achieve and few types of finite elements are known to guarantee it. We consider probably the simplest of them, the well known Bogner-Fox-Schmit rectangle [2], i.e., a rectangular C^1 element in two space dimensions.

Our MATLAB implementation is based on codes from [1, 6, 8]. The main focus of these papers were assemblies of finite element matrices and local element matrices were computed all at once by array operations and stored in multi-dimensional arrays (matrices). In this paper, we utilize underlying vectorization concepts without the particular interest in corresponding FEM matrices. We are primarily interested in explaining the construction of BFS elements and their applications leading to evaluations of energies. Herewith we provide more details on our recent implementations of C^1 models in nonlinear elastic models of solids [5, 7, 4].

The complementary software to this paper is available at

<https://www.mathworks.com/matlabcentral/fileexchange/71346>

for download and own testing.

*The work was supported by the Czech Science Foundation (GACR) through the grant GA18-03834S and GA17-04301S.

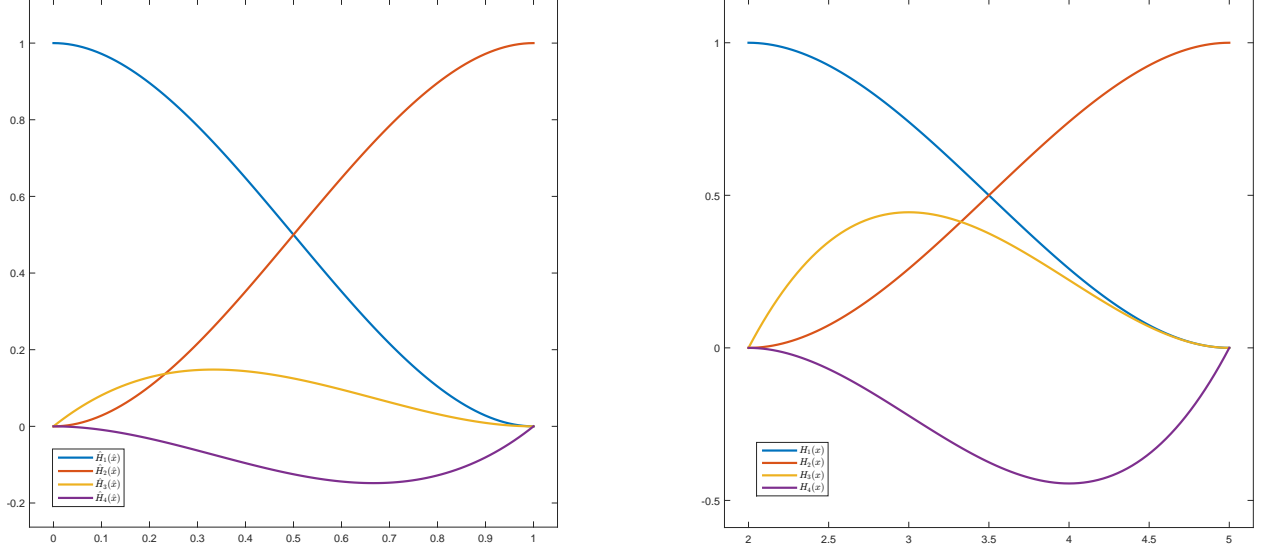


Figure 1: Reference basis functions $\hat{H}_i, i = 1, \dots, 4$ on $[0, 1]$ (left) and example of actual basis functions $H_i, i = 1, \dots, 4$ on $[a, b] = [2, 5]$ (right).

2 Construction of C^1 finite elements

2.1 Hermite element in 1D

We define four cubic polynomials

$$\begin{aligned}\hat{H}_1(\hat{x}) &:= 2\hat{x}^3 - 3\hat{x}^2 + 1, \\ \hat{H}_2(\hat{x}) &:= -2\hat{x}^3 + 3\hat{x}^2, \\ \hat{H}_3(\hat{x}) &:= \hat{x}^3 - 2\hat{x}^2 + \hat{x}, \\ \hat{H}_4(\hat{x}) &:= \hat{x}^3 - \hat{x}^2\end{aligned}\tag{1}$$

over a reference interval $\hat{I} := [0, 1]$ and can easily check the conditions:

$$\begin{aligned}\hat{H}_1(0) &= 1, & \hat{H}_1(1) &= 0, & \hat{H}_1'(0) &= 0, & \hat{H}_1'(1) &= 0, \\ \hat{H}_2(0) &= 0, & \hat{H}_2(1) &= 1, & \hat{H}_2'(0) &= 0, & \hat{H}_2'(1) &= 0, \\ \hat{H}_3(0) &= 0, & \hat{H}_3(1) &= 0, & \hat{H}_3'(0) &= 1, & \hat{H}_3'(1) &= 0, \\ \hat{H}_4(0) &= 0, & \hat{H}_4(1) &= 0, & \hat{H}_4'(0) &= 0, & \hat{H}_4'(1) &= 1,\end{aligned}\tag{2}$$

so only one value or derivative is equal to 1 and all other three values are equal to 0. These cubic functions create a finite element basis on \hat{I} .

More generally, we define for $x \in I := [a, b]$,

$$\begin{aligned}H_1(x) &:= \hat{H}_1(\hat{x}(x)), \\ H_2(x) &:= \hat{H}_2(\hat{x}(x)), \\ H_3(x) &:= h \hat{H}_3(\hat{x}(x)), \\ H_4(x) &:= h \hat{H}_4(\hat{x}(x)),\end{aligned}\tag{3}$$

where $\hat{x}(x) := (x - a)/h$ is an affine mapping from I to \hat{I} and h denotes the interval size $h := b - a$. These functions are also cubic polynomials and satisfy again the conditions (2) with function arguments

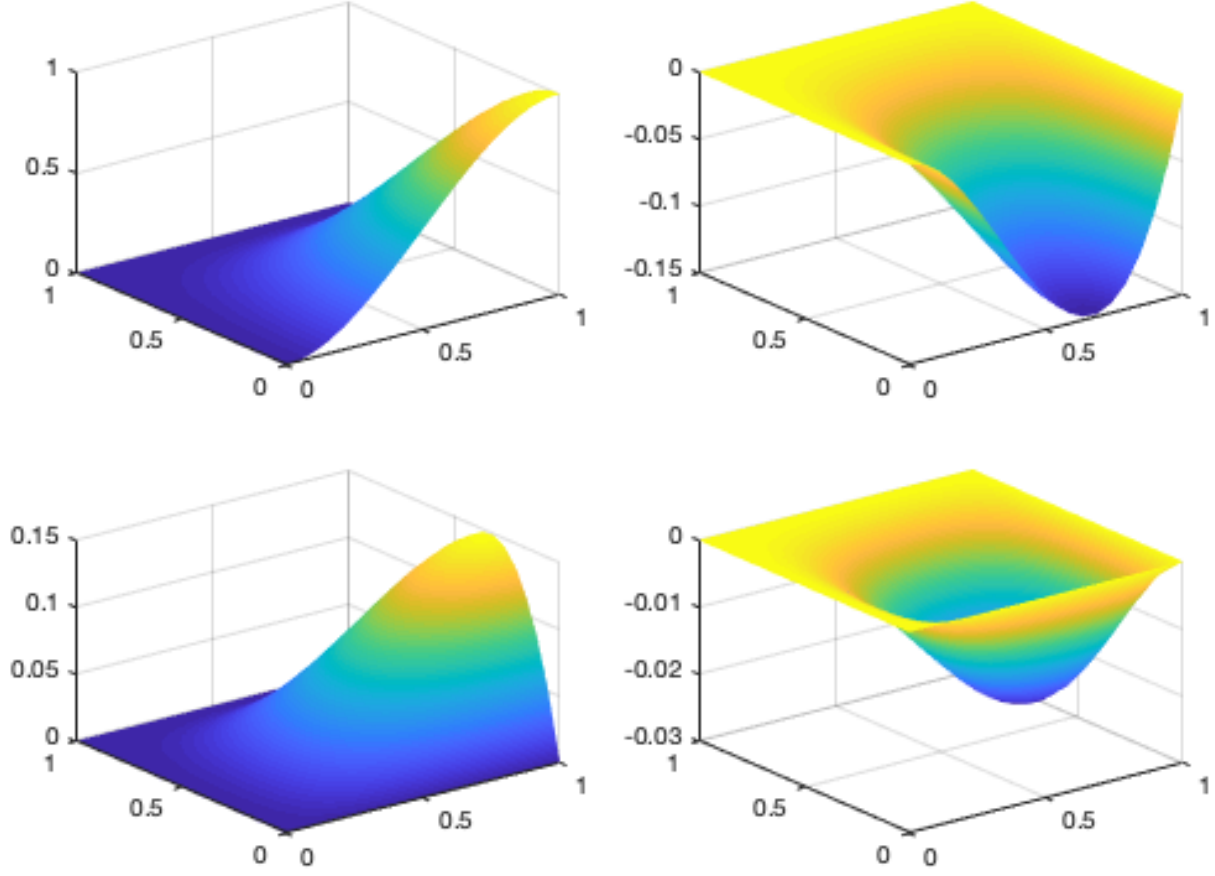


Figure 2: Bogner-Fox-Schmit basis functions $\hat{\varphi}_i(\hat{x}, \hat{y})$ for $i = 2$ (top left), $i = 6$ (top right), $i = 8$ (bottom left), $i = 13$ (bottom right) defined over a reference rectangle $\hat{R} = [0, 1] \times [0, 1]$.

0, 1 replaced by a, b . They create actual finite element basis which ensures C^1 continuity of finite element approximations. The chain rule provides higher order derivatives:

$$\begin{aligned}
 H'_1(x) &= \hat{H}'_1(\hat{x}) (1/h), & H''_1(x) &= \hat{H}''_1(\hat{x}) (1/h^2), \\
 H'_2(x) &= \hat{H}'_2(\hat{x}) (1/h), & H''_2(x) &= \hat{H}''_2(\hat{x}) (1/h^2), \\
 H'_3(x) &= \hat{H}'_3(\hat{x}), & H''_3(x) &= \hat{H}''_3(\hat{x}) (1/h), \\
 H'_4(x) &= \hat{H}'_4(\hat{x}), & H''_4(x) &= \hat{H}''_4(\hat{x}) (1/h).
 \end{aligned} \tag{4}$$

Example 1. Example of basis functions defined on reference and actual intervals are shown in Figure 1 and pictures can be reproduced by

```
draw_C1basis_1D
```

script located in the main folder.

2.2 Bogner-Fox-Schmit rectangular element in 2D

We consider a reference rectangle $\hat{R} := [0, 1] \times [0, 1]$ with nodes

$$\hat{N}_1 := [0, 0], \quad \hat{N}_2 := [1, 0], \quad \hat{N}_3 := [1, 1], \quad \hat{N}_4 := [0, 1].$$

Products of functions

$$\tilde{\varphi}_{j,k}(\hat{x}, \hat{y}) := \hat{H}_j(\hat{x}) \hat{H}_k(\hat{y}), \quad j, k = 1, \dots, 4$$

define 16 Bogner-Fox-Schmit (BFS) basis functions. For practical implementations, we reorder them

$$\hat{\varphi}_i(\hat{x}, \hat{y}) := \tilde{\varphi}_{j_i, k_i}(\hat{x}, \hat{y}), \quad i = 1, \dots, 16,$$

where sub-indices read

$$(j_i, k_i)_{i=1}^{16} = \begin{matrix} \{(1, 1), (2, 1), (2, 2), (1, 2), \\ (3, 1), (4, 1), (4, 2), (3, 2), \\ (1, 3), (2, 3), (2, 4), (1, 4), \\ (3, 3), (4, 3), (4, 4), (3, 4)\}. \end{matrix} \quad (5)$$

With this ordering, a finite element approximation $v \in C^1(\hat{R})$ rewrites as a linear combination

$$v(\hat{x}, \hat{y}) = \sum_{i=1}^{16} v_i \hat{\varphi}_i(\hat{x}, \hat{y}),$$

where:

- the first 4 coefficients specify v at nodes $\hat{N}_1, \dots, \hat{N}_4$,
- the second 4 coefficients specify $\frac{\partial v}{\partial x}$ at nodes $\hat{N}_1, \dots, \hat{N}_4$,
- the third 4 coefficients specify $\frac{\partial v}{\partial y}$ at nodes $\hat{N}_1, \dots, \hat{N}_4$,
- the last 4 coefficients specify $\frac{\partial^2 v}{\partial x \partial y}$ at nodes $\hat{N}_1, \dots, \hat{N}_4$.

For a general rectangle $R := [a, b] \times [c, d]$, we define an affine mapping

$$(\hat{x}, \hat{y})(x, y) := ((x - a)/h_x, (y - c)/h_y),$$

from R to \hat{R} , where the rectangular lengths are $h_x := b - a$, $h_y := d - c$. Based on (4), higher order derivatives can be derived as well. All basis functions are evaluated in

```
[shape] = shapefun (point, etype, h)
```

function and their derivatives up to order 2 in

```
[dshape] = shapeder (point, etype, h)
```

function. For BFS elements, we have to set

```
etype='C1'
```

and a vector of rectangular lengths

```
h=[hx, hy]
```

The matrix `point` then contains a set of (quadrature) points $\hat{x} \in \hat{R}$, at which functions are practically evaluated. The functions are vectorized and store their outputs in multi-dimensional arrays.

Example 2. *Four (out of sixteen) reference basis functions corresponding to the node \hat{N}_2 are shown in Figure 2 and pictures can be reproduced by*

```
draw_C1basis_2D
```

script located in the main folder.

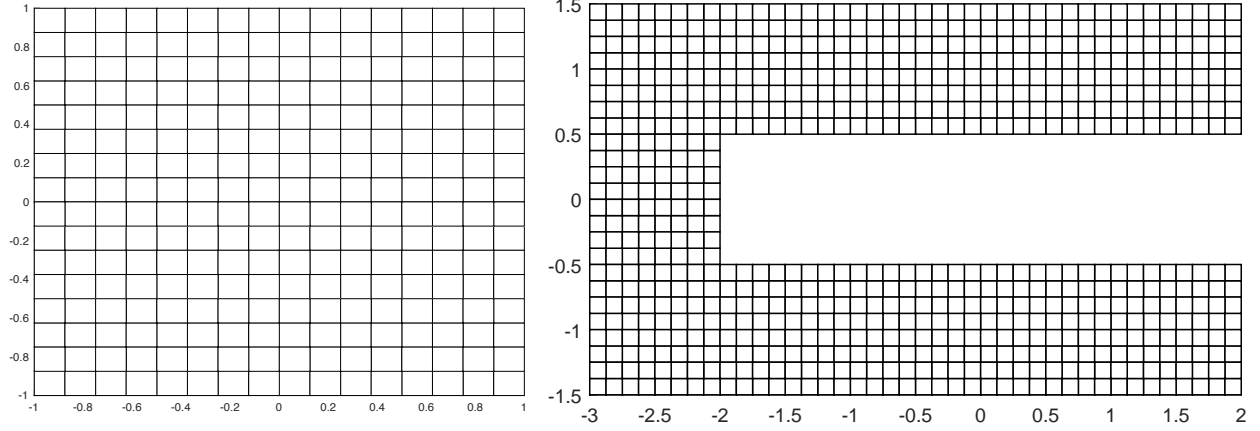


Figure 3: Examples of a triangulation in rectangles: of a square domain (left) and of a pincers domain (right) taken from [7] and used for nonlinear elasticity simulations satisfying a non-selfpenetration condition.

2.3 Functions representation and visualization

Let us assume a triangulation $\mathcal{T}(\Omega)$ into rectangles of a domain Ω . In correspondence with our implementation, we additionally assume that all rectangles are of the same size, i.e., with lengths $h_x, h_y > 0$. Examples of $\mathcal{T}(\Omega)$ are given in Figure 3.

Let \mathcal{N} denotes the set of all rectangular nodes and $|\mathcal{N}| := n$ the number of them. A C^1 function $v \in \mathcal{T}(\Omega)$ is represented in BSF basis by a matrix

$$V = \begin{pmatrix} v(N_1), & \frac{\partial v}{\partial x}(N_1), & \frac{\partial v}{\partial y}(N_1), & \frac{\partial^2 v}{\partial x \partial y}(N_1) \\ \vdots & \vdots & \vdots & \vdots \\ v(N_n), & \frac{\partial v}{\partial x}(N_n), & \frac{\partial v}{\partial y}(N_n), & \frac{\partial^2 v}{\partial x \partial y}(N_n) \end{pmatrix}$$

containing values of $v, \frac{\partial v}{\partial x}, \frac{\partial v}{\partial y}, \frac{\partial^2 v}{\partial x \partial y}$ in all nodes of $\mathcal{T}(\Omega)$. In the spirit of the finite element method, values of v on each rectangle $T \in \mathcal{T}(\Omega)$ are obtained by an affine mapping to the reference element \hat{R} . Our implementations allows to evaluate and visualize continuous fields

$$v, \frac{\partial v}{\partial x}, \frac{\partial v}{\partial y}, \frac{\partial^2 v}{\partial x \partial y}$$

and also two additional generally discontinuous fields

$$\frac{\partial^2 v}{\partial x^2}, \frac{\partial^2 v}{\partial y^2}.$$

Example 3. We consider a function

$$v(x, y) = (1 - x^2)^2(1 - y^2)^2 \quad (6)$$

on the domain $\Omega = (-1, 1)^2$. This function was also used in [4] as an initial vertical displacement in a time-dependent simulation of viscous von Kármán plates. To represent v in terms of BFS elements, we additionally need to know values of

$$\frac{\partial v}{\partial x}(x, y) = 2(1 - x^2)(1 - y^2)^2 \quad (7)$$

$$\frac{\partial v}{\partial y}(x, y) = 2(1 - x^2)^2(1 - y^2) \quad (8)$$

$$\frac{\partial^2 v}{\partial x \partial y}(x, y) = 4(1 - x^2)(1 - y^2) \quad (9)$$

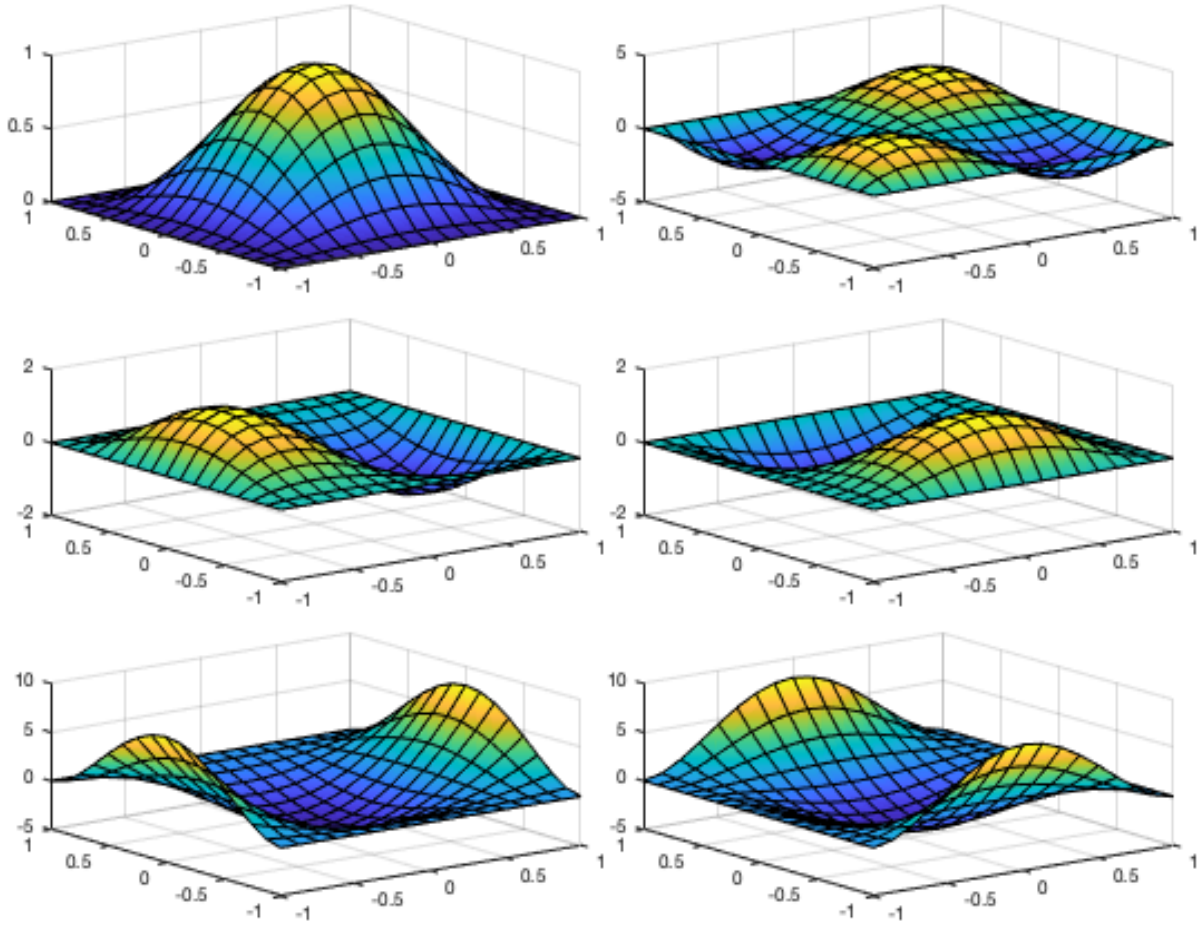


Figure 4: A function $v(x, y) = (1 - x^2)^2(1 - y^2)^2$ on $\Omega = (-1, 1)^2$ approximated in terms of BSF elements. Separate pictures show: v (top left), $\frac{\partial^2 v}{\partial x \partial y}$ (top right), $\frac{\partial v}{\partial x}$ (middle left), $\frac{\partial v}{\partial y}$ (middle right), $\frac{\partial^2 v}{\partial x^2}$ (bottom left), $\frac{\partial^2 v}{\partial y^2}$ (bottom right).

in nodes of a rectangular mesh $\mathcal{T}(\Omega)$. The function and its derivatives up to the order two are shown in Figure 4. All pictures can be reproduced by

`draw_C1example_2D`

script located in the main folder.

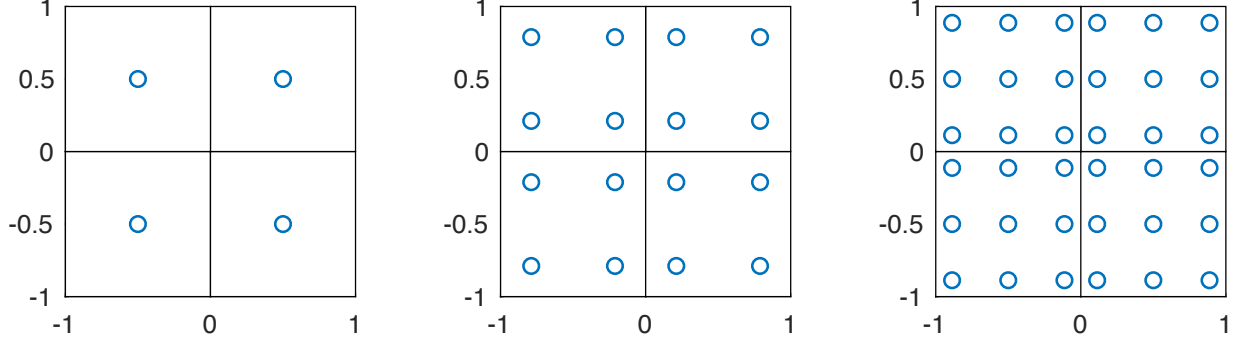


Figure 5: Quadrature rules with 1, 4 and 9 Gauss points shown on actual rectangles of a square domain with 4 rectangles.

2.4 Numerical integration

Various energy formulations include evaluations of integrals of the types

$$||v||^2 : = \int_{\Omega} |v(x, y)|^2 dx dy, \quad (10)$$

$$||\nabla v||^2 : = \int_{\Omega} |\nabla v(x, y)|^2 dx dy, \quad (11)$$

$$||\nabla^2 v||^2 : = \int_{\Omega} |\nabla^2 v(x, y)|^2 dx dy, \quad (12)$$

$$(f, v) : = \int_{\Omega} f v dx dy, \quad (13)$$

where $v \in H^2(\Omega)$ and $f \in L^2(\Omega)$ is given. The expression

$$(||v||^2 + ||\nabla v||^2 + ||\nabla^2 v||^2)^{1/2}$$

then defines the full norm in the Sobolev space $H^2(\Omega)$. For v represented in the BFS basis we can evaluate above mentioned integrals numerically by quadrature rules. Our implementation provides three different rules with 1, 4 or 9 Gauss points. Each quadrature rule is defined by coordinates of all Gauss points and their weights.

Example 4. *Used Gauss points are displayed in Figure 5 and all pictures can be reproduced by*

`draw_ips`

script located in the main folder.

Since integrals are evaluated in each rectangle separately, it is possible to compute and visualize averaged densities over each rectangle.

Example 5. *An analytical integration for the function v from (6) and $f = 1$ reveals that*

$$\begin{aligned} ||v||^2 &= 65536/99225 \approx 0.660478710002520, \\ ||\nabla v||^2 &= 131072/33075 \approx 3.962872260015117, \\ ||\nabla^2 v||^2 &= 65536/1225 \approx 53.498775510204084, \\ (f, v) &= 256/225 \approx 1.1377777777777778. \end{aligned}$$

Figures 6 and 7 depict the convergence of numerical quadratures to these values and resulting averages densities. All pictures can be reproduced by

`start_evaluate`

script located in the main folder.

References

- [1] Immanuel Anjam, Jan Valdman: *Fast MATLAB assembly of FEM matrices in 2D and 3D: edge elements*, Applied Mathematics and Computation, 2015, 267, 252–263.
- [2] F.K. Bogner, R.L. Fox and L.A. Schmit: The generation of inter-element compatible stiffness and mass matrices by the use of interpolation formulas, *Proceedings of the Conference on Matrix Methods in Structural Mechanics*, (1965), 397–444.
- [3] P.G. Ciarlet: *The Finite Element Method for Elliptic Problems*, SIAM, Philadelphia, 2002.
- [4] Manuel Friedrich, Martin Kružík, Jan Valdman: Numerical approximation of von Kármán viscoelastic plates, *Discrete and Continuous Dynamical Systems - Series S* (submitted).
- [5] S. Forest: *Micromorphic approach for gradient elasticity, viscoplasticity, and damage*, J. Eng. Mech. 135 (2009) 117.
- [6] P. Harasim, J. Valdman: Verification of functional a posteriori error estimates for an obstacle problem in 2D, *Kybernetika*, **50** (6) (2014), 978–1002.
- [7] Stefan Krömer, Jan Valdman: *Global injectivity in second-gradient Nonlinear Elasticity and its approximation with penalty terms*, Mathematics and Mechanics of Solids (submitted).
- [8] Talal Rahman, Jan Valdman: *Fast MATLAB assembly of FEM matrices in 2D and 3D: nodal elements*, Applied Mathematics and Computation, 2013, 219, 7151–7158.

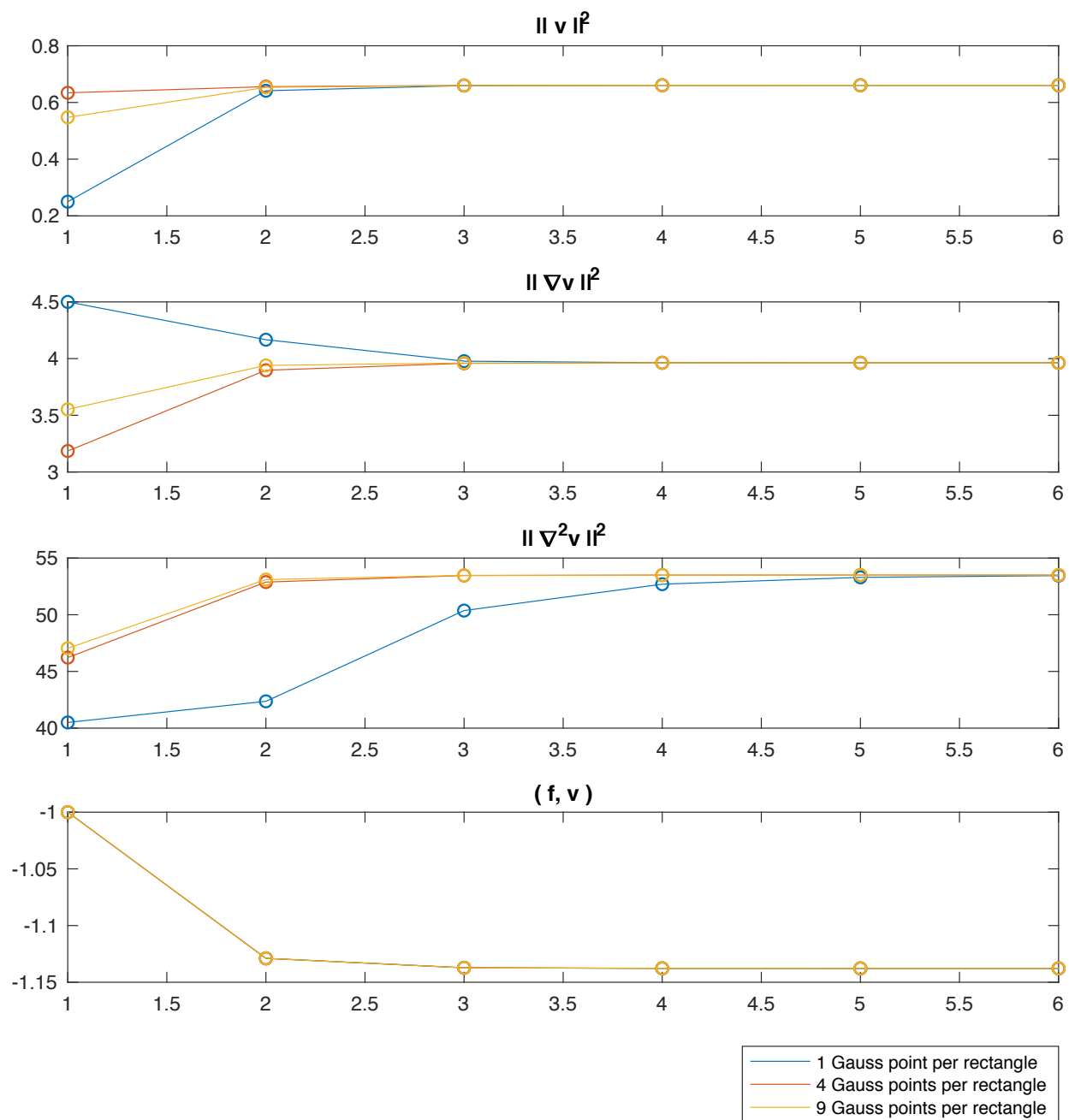


Figure 6: Values of integrals for various levels of uniform refinements using three different quadrature rules.

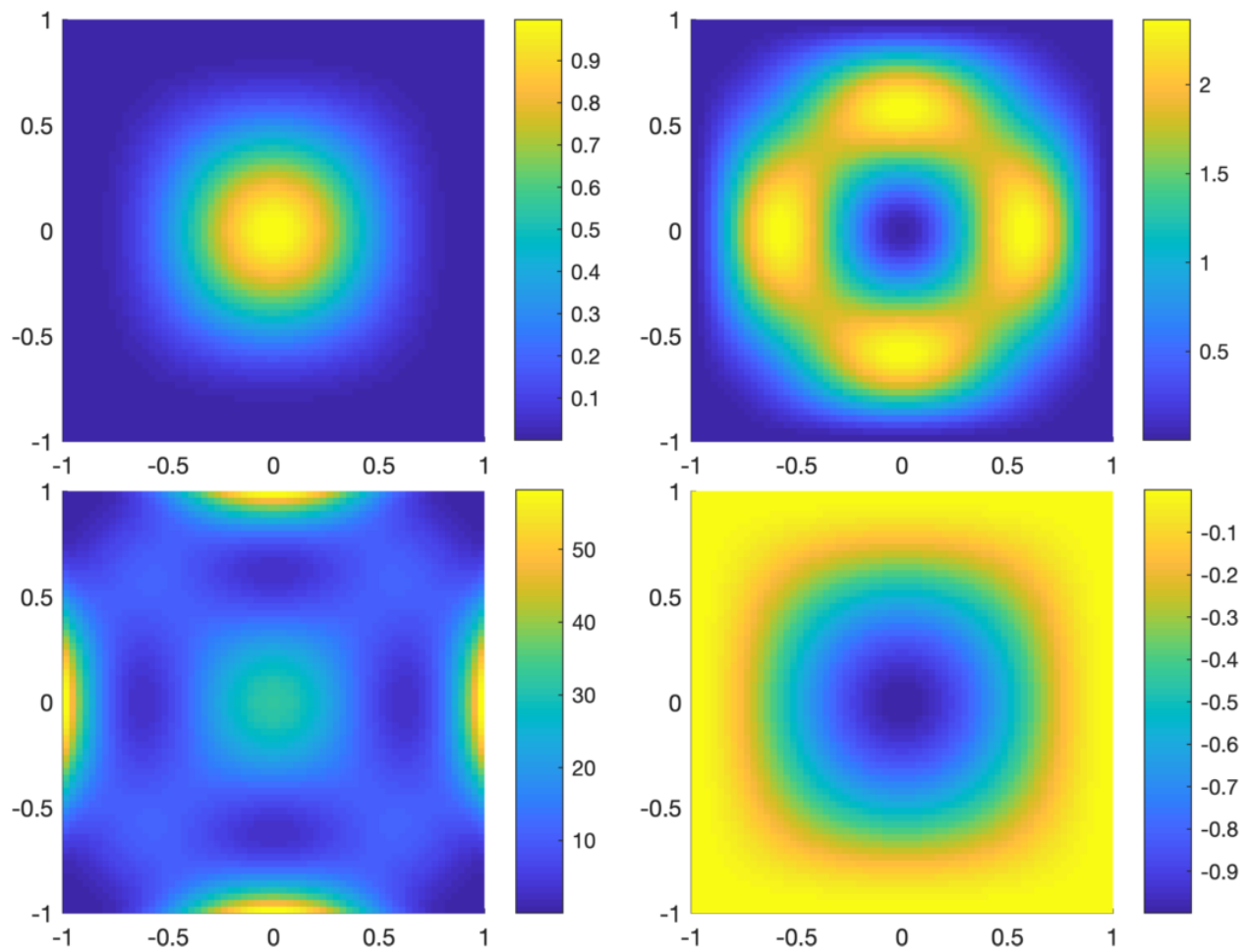


Figure 7: Averaged densities over each rectangle: $\|v\|^2$ (top left), $\|\nabla v\|^2$ (top right), $\|\nabla^2 v\|^2$ (bottom left), (f, v) (bottom right).